Numerical Simulation of the Thermal Performance of Four Concentrating Collectors with Bifacial PV Cells

Miguel Lança[1], João Gomes[2] and Abolfazl Hayati[2]

[1] Instituto Superior Técnico, Lisbon University, Portugal

[2] University of Gävle, Sweden

Abstract

Bifacial photovoltaic cells can produce electricity from the incoming solar radiation on both sides. Used in combination with concentrating solar technology, bifacial photovoltaic cells can see its electrical output further augmented, thus decreasing the cost per kWh. It is known, however, that the efficiency reduction when these cells are exposed to increased temperatures is a relevant factor. This can happen, for example, when they are mounted on a glassed collector or receiver. In this study, a thermal analysis is carried out on four prototypes of concentrating collectors with bifacial PV cells. Results show that, as expected, when glass and gables are removed from the collector, much better heat dissipation is achieved, thus resulting in favorable cell operation conditions.

Keywords: PV cells, concentrators, reflector geometry, CFD, glass receiver

1. Introduction

Concentrators are a route to achieve high photovoltaic cell efficiencies as well as cost reduction. This reduces land utilization as well as area related costs (Mehrdad et al, 2014). In Photovoltaic–Thermal (PVT) technology, for systems with and without concentration, the use of glass cover on the flat-plate hybrid solar collector is common. This enhances the thermal output but not the electric. While a solar thermal panel must be able to retain heat in order to reach high operating efficiencies, a photovoltaic panel behavior is the opposite; the efficiency is reduced with the temperatures increase. Several means for temperature control of the PV cell collector have been studied (Alizadeh et al, 2018; Du, 2017; Kasaeian et al., 2017; Wu et al., 2018).

This paper conducts thermal analysis based on Computational fluid dynamics (CFD) simulations to four prototype Parabolic Concentrators collectors with bifacial PV cells encapsulated in a glass receiver.

Thermal analysis of PVT systems is frequently encountered in literature. Sun and Shi (2009) studied the thermal performance of a C-PVT collector. The results have shown that the solar radiation intensity can be higher than 1200 W/m^2 in most area of the cell surface. The temperature of the air and cell surface was reported to rise along the length of the system. The authors have concluded that the receiver temperature is related to both air mass flow and length, as well as solar radiation and outdoor temperature. Li et al. (2016) studied the influence of the incidence angle on the temperature of the cover and back glass and also on the cell silicone temperature. They performed experiments and CFD calculations for 0º, 10º, 20º, 30º and 40º incidences. Crossed Parabolic was the type of concentrator analyzed. Gomes et al. (2012) carried out tests on three prototypes of CPC collectors with bifacial PV cells. Results showed a cell temperature of 88ºC on a glass-covered outdoor installed CPC collector on a sunny day with 28ºC of outside temperature. The dependence of electrical efficiency on temperature was reported to be -0.51 %/K.

2. The collector prototypes

The study compares four concentrating bifacial PV collectors designs described in table 1.

doi:10.18086/eurosun2018.02.25 Available at http://proceedings.ises.org

Tab. 1 – A cross-section view (plane *zx*) of the four cases studied and each one´s composition (not to scale).

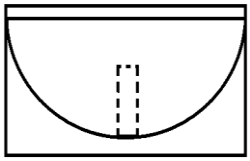	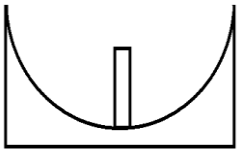	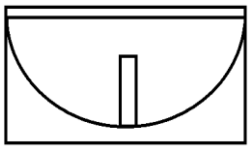	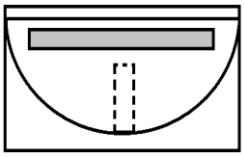
Case 1: Totally covered - Includes the box structure, side gables, glass cover, glass receiver (dotted line) and reflector.	**Case 2: Totally uncovered** - Includes the box structure, glass receiver and reflector but no glass cover, nor side gables	**Case 3: Partially covered** - Includes the box structure, glass cover, glass receiver and reflector but not the side gable.	**Case 4: Partially uncovered with a ventilation slot** - Includes the box structure, side gables with ventilation slot (in gray in the figure), glass cover, glass receiver (dotted line) and reflector.

All above cases have different heat performance, meaning that the solar cells will operate at different temperatures. Therefore all cases were compared on air velocity, air and collector temperature and heat fluxes. Figure 1 shows an overall picture of the complete solar collector.

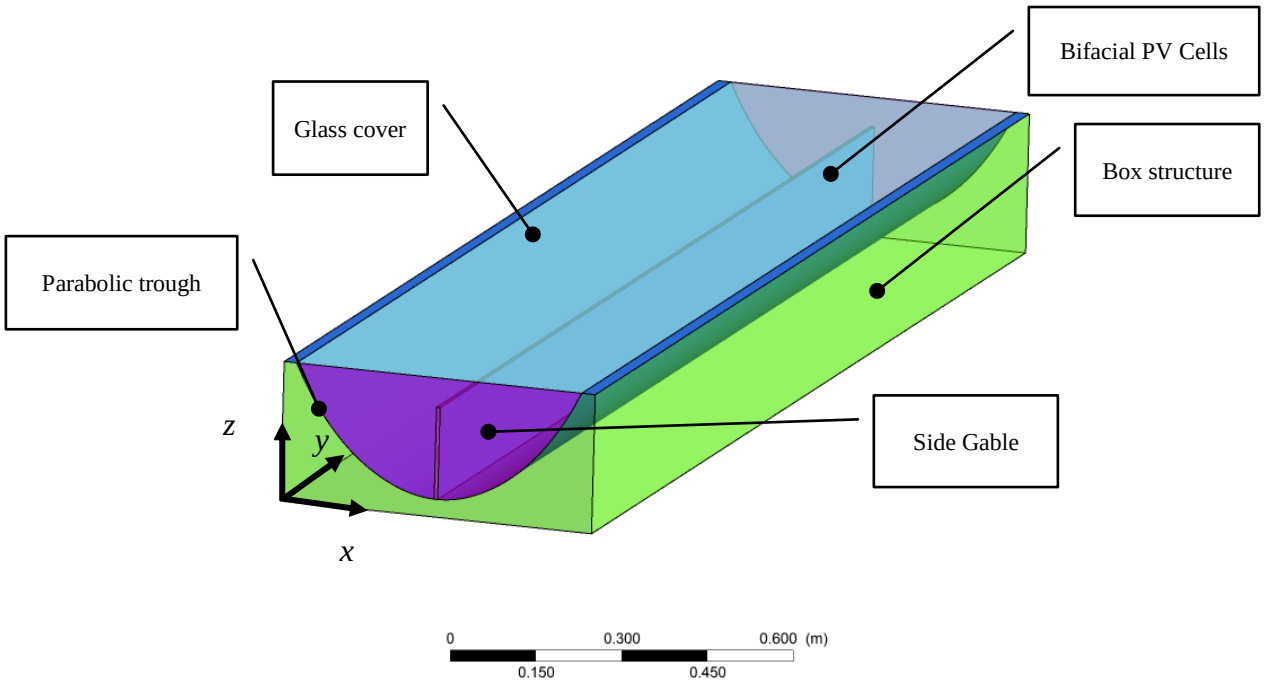

Fig. 1: Model of the glass covered concentrating collector studied.

The collector dimensions are 600 mm × 2250 mm × 250 mm (*x*,*y*,*z*). The glass over the collector and of the receiver is a 4 mm glass with a weighted solar light transmittance of 95% at 600 nm wavelength. The parabolic trough is made of 2 mm aluminum with a weighted solar light reflectivity of 93%. The receiver comprises a set of 4 layers: a 0.5mm cell between 2 coatings of 0.5 mm silicone, and a 4 mm glass attached to one of the sides. A numerical study is carried out using a commercial CFD tool, ANSYS FLUENT. The simulations take in to account the physics when the collector is operating. Energy, continuity, momentum, radiation, turbulence models and boundary conditions are set in order to give the simulation the correct approximation to the lab and field operation. Each mathematical model is explained in detail in section 3. Figure 2 is a heat flow network

used to describe the thermal analysis used here.

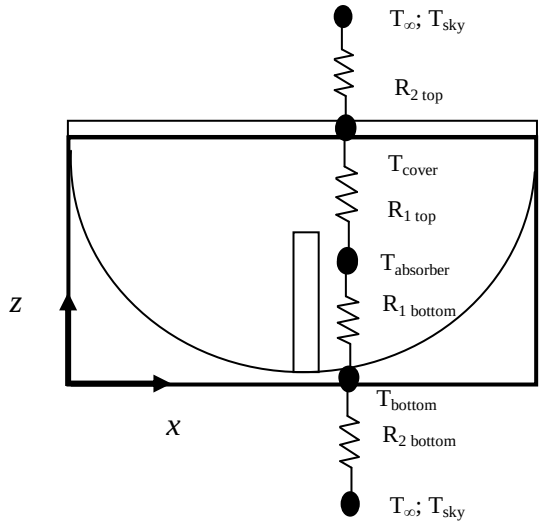

Fig. 2: Equivalent heat flow network for the covered collector.

The overall energy balance for the transient state is given by Eq. 1:

$$G_{collector} A_{absorber} \tau_{cover} \alpha_{absorber} = q_{loss} + \frac{de_{collector}}{dt} \quad \text{(eq. 1)}$$

Where $G_{collector}$ is the solar irradiation striking the collector, $A_{abosrber}$ is the area of the collector, τ_{cover} is the glass transmittance and $\alpha_{absorber}$ the receiver absorptance. q_{loss} represent the heat loss due to conduction, convection and radiation and the last term of the second member of the equation denote the transient term. Assuming steady-state and one-dimensional heat analysis, q_{loss} can be calculated as:

$$q_{loss} = \frac{T_{absorber} - T_{\infty}}{R_{total}} \quad \text{(eq. 2)}$$

And each of the convection/radiation combined resistance components as:

$$\frac{1}{R_{total}} = \frac{1}{R_{1\,top} + R_{2\,top}} + \frac{1}{R_{1\,bottom} + R_{2\,bottom}} \quad \text{(eq. 3)}$$

Where R_{1top} is a parallel resistance electric analog circuit, consisting of the convection and radiating components taking place between the receiver and the cavity, and R_{2top} representing the combination between the two resistances that form the radiating and convective heat transfer that is being processed between the glass and the exterior medium. The same principle is applied to the bottom, where $R_{1bottom}$ and $R_{2bottom}$ designate the resistances that form the collector bottom surface – convection and radiation, respectively, between the receiver, the cavity and the outer case with the environment.

This study compares collectors with or without glass cover as well as with or without side different types of side gable. The expressions treated above are intended to represent the first case. When the receiver is uncovered, a different thermal approach needs to be taken. There is no need to consider the transmittance of the glass and the radiative and convective components between the receiver and the cavity. R_{1top} and R_{2top} are in this case, transformed in a single thermal resistance, say $R_{top.}$

3. Numerical methods

Exact or approximate analytical solutions for the temperature and velocity vectors can only be obtained for simple problems and particular boundary conditions.
Since the 1960s, computational fluid dynamics (CFD) has seen an increase in popularity in the aerospace, thermal and biomedical sciences sectors, to name a few. Nowadays, with the mass use of powerful processing computers, it is possible to obtain very good levels of mesh refinement on three dimensions models. These technological improvements coupled with the evolution of knowledge about the theory of turbulence, the simulations today produce results of extraordinary accuracy (Li, 2007).
In CFD modeling, several equations are solved, i.e. momentum, energy, turbulence, radiation, and concentration, in order to find out how are the boundary conditions transported to the interior of the domain according to the mechanisms of diffusion, convection, and chemical reactions.
In this study, the objective of the CFD simulations is the prediction for the thermal variables when a concentrating PV collector is exposed to peak solar conditions. The simulations resulted from the resolution of the equations referred to a steady and incompressible regime, using the three dimensions in space. Turbulence models were employed according to the RANS - Reynolds Average Navier Stokes method. The effects of radiation, as well as buoyancy, were taken into account.

Errors and uncertainties are part of computational simulations. For this reason, it is essential to develop methods to quantify the confidence level of the results, (Versteeg and Malalasekera, 2007). A set of techniques allows one to solve the equations correctly and, at the same time, also that the right equations are being solved. Residual error, rounding errors or those inherent to the discretization process are some examples. Rounding errors can be quantified by running, for example, two simulations, each with a different selected precision level, and comparing the results. Fluent software classifies these two levels as single precision and double precision. Residual errors, in turn, can be evaluated by comparing the evolution of residuals of one or more variables intrinsic to the study, such as heat flux or temperature. The greater or lesser oscillation of these quantities residuals throughout the iterative process indicates how far away is the actual solution from the final solution. The error inherent on the discretization of equations will depend on the accuracy of the approximation of the differential equations to the arithmetic ones, namely to the truncated terms of higher order in the development of the Taylor series. Since the equations in the differential form are valid at any point in the domain, while the discrete solution is valid only at the points or nodes where the model was divided, it follows that this type of error is usually affected by the time step used in transient simulations and by the quality of the mesh. In this case, this error can be quantified by running simulations in which, for example, the mesh size is varied from case to case.

While errors in CFD simulations are known to the user that can to some extent control them, the magnitude and origin of the uncertainties involved in such calculations are unknown, e.g. geometry, properties of materials used, boundary conditions, turbulence or radiation models.

3.1. *CFD Set-up*

3.1.1. *Turbulence*

Studies have pointed out that the accuracy in the prediction of turbulent flow behavior is a consequence of the accuracy of the turbulence models used in this same forecast (Spentzos, 2005).

Turbulence is a complex problem. It affects mainly the numerical analysis, although it might also introduce uncertainties in the experimental analysis as well. While the movement of the fluid is continuous, in reality, the motion of the particles is not ordered. When this occurs velocity vectors are affected and these fluctuations influence also the transport of the energy, momentum, and concentration-related variables. Turbulence modeling implies that the Navier-Stokes equations will include the product of the floating components - the so-called Reynolds stress. Closing strategies emerged as a way of solving the new system of equations then generated. Turbulence models may have one or more equations. For the selection of the model to be used, the degree of turbulence evolved needs to be known in order that an acceptable numerical approximation can be obtained.

3.1.1.1. The k-ε model

Widely used in studies of fluid mechanics and heat transfer this model combines relative robustness of results and accuracy without being computally expensive. It is a semi-empirical model of two equations in which the turbulent transport variables are the turbulent kinetic energy (k) and the dissipation rate (ε). The first is defined based on an exact solution whereas the second on empirical solutions which result from the observation of physical phenomena. In this study the standard k- ε model was used and the following constants were adopted:

Tab. 2: constants used in the k- ε turbulence model

Constant	Value
C_{μ}	0,09
$C_{1\varepsilon}$	1,44
$C_{2\varepsilon}$	1,92

Standard wall functions were also used when the characterization of the flow near the wall.

3.2. Buoyancy

In the presence of heat transfer to the air, a variation of its density will occur as a consequence of its heating. The gravitational force will act under different intensities, promoting the movement of the particles. Natural convection is possible to be modeled numerically by Fluent software. In those circumstances, the Boussinesq approach is normally adopted. This approximation treats density as constant in all but in the momentum equation where the density property will be expressed as a function of temperature:

$$(\rho - \rho_0)g \approx -\rho_0 \beta(T-T_0)g \qquad \text{(eq.4)}$$

Where ρ_0 designates the reference air density and T_0 is the temperature under study, β the air expansion coefficient and g the gravitational acceleration. This approach presents results with acceptable deviations as long as the variations in the air temperature are reduced, that is when $\beta (T-T_0) << 1$. For the buoyancy modeling to be implemented the gravitational acceleration also has to be introduced, which in this case will act in the direction of the z-axis with a value of -9.81 m/s^2.

3.3. Boundary conditions

The definition of boundary conditions constitutes an important part of the formulation of any problem to be solved by a CFD code, (Versteeg and Malalasekera, 2007).

The boundary conditions were defined in order to describe appropriately the physical conditions. In this work, 3 types of boundary conditions were chosen: wall, pressure-inlet and pressure-outlet whether the collector is covered or uncovered with the glass. Each collector boundary condition is defined in table 3.

Tab. 3: List of boundary conditions assigned to each surface of the prototypes calculated. LW stands for Law of the Wall.

	Type of boundary condition Case 1/ Case 2/ Case 3/ Case 4
Glass (plane z=250 mm)	LW/pressure outlet/ LW/ LW
East gable (plane y=0 mm)	LW/pressure inlet/pressure inlet/pressure inlet+LW
West gable (plane y=2250 mm)	LW/pressure inlet/pressure outlet/pressure outlet+LW
Box structure	law of the wall

The “pressure outlet” was chosen (with gauge pressure taken equal to zero) to define the static pressure at the flow outlets. In this case, backflow total temperature is taken equal to outdoor temperature.
The “wall” boundary condition is used to define the fluid-solid interface. In this option, for viscous flows, the no-slip boundary condition is enforced at the wall and defined as stationary. The remaining external walls were defined considering losses by convection and radiation, according to the properties and thickness of a virtual

wall. In more than one surface the boundary conditions are classified as convection type which implies the definition of a medium temperature and an external convection coefficient. The latter was calculated analytically considering the air properties at an exterior temperature of 25ºC. The calculated convective coefficient also accounts for the effects of radiation on heat exchanges between the model and the surrounding surfaces or the sky and can, therefore, be referred to as the combined convection coefficient.

The heat conduction is also calculated by Fluent software on solid domains. For this purpose, a mesh was created in those regions. In this study, for reasons of speed of calculation, it was decided to be applied only on the receiver. In the case of glass walls and gable, a mesh was not generated for a resource-saving reason, but rather defined a thickness and specified a material.

3.4. Radiation

In the presence of heat transfer by natural convection the radiation component may represent a significant fraction of the heat transferred (Çengel, 2002). Therefore, the radiation emitted by the bodies will be absorbed by the surrounding surfaces conditioning the final balance of energy.

3.4.1. The surface to surface (S2S) model.

The surface-to-surface radiation model is typically used to model radiative heat transfer in non-participating mediums. Thus, it is assumed that the heat exchanges by radiation only occur between surfaces. This depends on their area, the distance that separates them and orientation, as well as their optical properties. The interaction between surfaces is given by the calculation of the view factor carried out automatically by the software. The S2S model assumes that all surfaces are diffuse and gray. In this study, the surfaces were also considered opaque except for the top glass. The biggest advantage of this model is its simplicity and the reduction of resources required for not taking into account any absorption, emission, or scattering of radiation by the filling medium, thus, it is appropriate for this problem.

The radiosity of a given surface J_s is the sum of the radiation energy E_s emitted by the surface s plus the total energy reflected by the same surface:

$$J_s = E_s + \rho_s \sum_{r=1}^{N} F_{sr} J_r \qquad \text{(eq. 5)}$$

Where ρ_s is the reflectance of the surface, F_{sr} is the view factor between the r surrounding surfaces and the one considered. As compared to other radiation models, the S2S model is solved by a fast direct method, although the view factor calculation itself is CPU-intensive. The storage and memory requirements increase very rapidly as the number of surface faces increases. To save calculation time, some of the surfaces can be merged into a unique group. In this study, the view factor was calculated considering every surface individually since the calculation time took about 10 minutes.

3.4.2. The solar model

The CFD code used enables the calculation of a heat source coming from the sun to predict the effects on the domain. This is accomplished by defining a beam that is modeled using the sun position vector and illumination parameters. The resulting heat flux is coupled to the calculation via a source term in the energy equation. A two-band spectral model is used for direct solar illumination and accounts for separate material properties in the visible and infrared bands. A single-band hemispherical-averaged spectral model is used for diffuse radiation. Opaque materials like the gable are characterized in terms of two-band absorptance. A semi-transparent material as the covering-glass requires specification of absorptance and transmittance.

Two options are available for the model: solar ray tracing and Discrete Ordinates irradiation. The simulations were carried out using the solar ray tracing method. Inputs of 1000 W/m^2 of direct radiation, as well as 100 W/m^2 of diffuse radiation, were considered. The sun direction vector was taken as pointing along z-axis only. Therefore the model assumes the incident solar radiation is striking the collector perpendicularly.

3.5. Grid generation

The mesh used comprises nearly 2 000 000 elements. The zones where higher velocity gradients are expected have been refined. At the same time, the mesh generation topology avoids sudden transition between elements of different sizes. An overall look of the mesh is represented in fig 3. The effect of mesh size reduction on the results obtained was investigated. Thus, several simulations were made maintaining the same geometry of the model but varying the number of mesh elements. It has been reported that for different mesh sizes, the calculated values of heat fluxes in the gable and air temperature at the receiver also varied considerably. On the other hand, it was found that the solution found difficulties converging or did not converge at all, below a minimum number of elements - around 200 000. On the contrary, when the number of elements was increased, the asymptotic evolution of the results took place. This sensitivity analysis served to optimize the mesh when trying to reach a compromise between the results accuracy and the calculation time. The mesh generation software used also provides quantitative geometric parameters of the mesh such as orthogonal quality and asymmetry. The overall mesh quality was checked and compared with the range of values indicative of a good overall quality - near 1 for orthogonal quality and 0 for asymmetry.

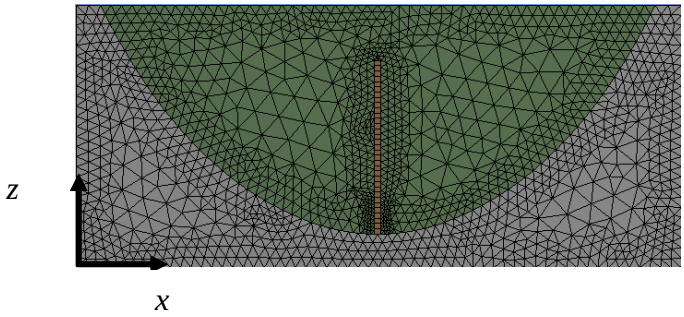

Fig. 3 – Mesh used in the calculations taken at the plane y=1000 mm.

3.6. Solver settings

The 3-D model was incorporated on Fluent software release 14.0. Momentum, energy, radiation and turbulence equations were calculated. The solver general settings were defined as an incompressible steady regime. The pressure-velocity coupling was determined by the algorithm PISO - Pressure Implicit with Splitting of Operators. The discretization of the momentum, energy and turbulence equations was processed using second-order upwind type numerical schemes.

4. Results and discussion

4.1 Case 1 – Totally Covered

The temperature and heat flux contours, as well as the velocity vectors for the covered collector case, are shown in Fig. 4. The highest air temperature is reported in the cavity between the glass and the receiver, which ranges between 100 and 130 °C, at the same time that the receiver reaches 150ºC. Of all the cases studied, this is the one that presents the highest temperatures in both the receiver and the surrounding zone, as expected, because of the greenhouse effect created by the presence of the glass. The cavity delimited by the box structure has lower temperatures than the upper zone - between 61 and 140 °C. The air in the base surface of the collector as well as near the walls is colder than the rest of the collector due to the losses that occur by convection and radiation between the collector walls and the environment. Also in the glass vicinity, it can be verified that there is a zone of transition between the highest temperatures of the air and the colder glass surface that form the thermal boundary layer. This collector presents the most severe operating conditions for the PV cells.

The velocity vector field shows the formation of two vortexes one on each side of the receiver. This is due to the temperature differences between this component and the rest of the surrounding air as it has been observed in temperature analysis. Highest velocity gradients happen near the walls (glass, receiver and reflector) especially at the top of the receiver and in the upper part of the reflector. Values between 0.02 and 0.17 m/s are encountered. Total heat fluxes (convective and radiative) contours reach 720 W/m^2 maximum and indicate that

higher losses occur in the glass. This can be explained due to the high air temperatures at these points that lead to greater heat exchanges with the environment.

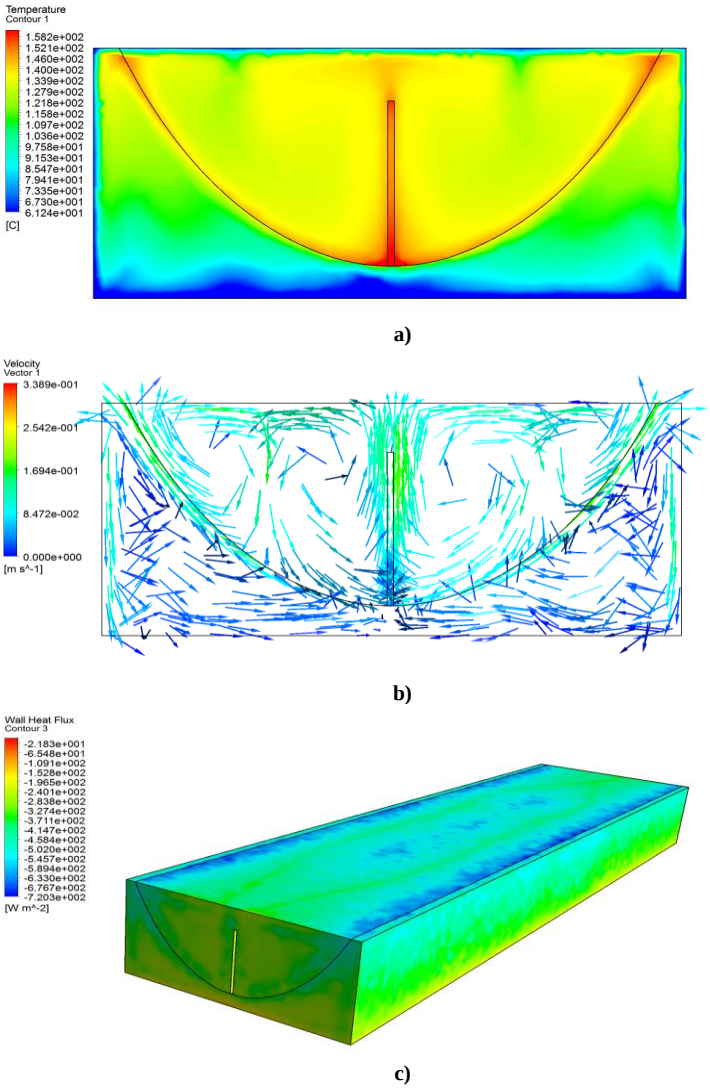

Fig. 4 – Calculated temperature contours (a) and velocity vectors (b) at the plane y=1000 mm and heat flux (c) contours for case 2.

4.2 Case 2 – Totally uncovered (no side gables nor top glass)

Presented data suggest a clear reduction on air and receiver temperatures compared to the covered collector case. Values close to ambient temperature are encountered around the receiver and this is working at 79ºC at most, with the majority of its interior below 61ºC. The absence of the glass cover makes the cooling of the receiver more efficient, thus decreasing the overall temperatures. There is a 5 K temperature difference between the bottom of the collector and the outside air, which indicates a less intense heat transfer rate in this region compared to the covered case. The overall receiver and air temperatures were the lowest of all 4 cases calculated. Since the fact that there is no glass, mass transfer is allowed which contributes to the cell temperature regulation.

The calculated velocity vectors indicate a clear direction of the flow from the exterior to the interior of the cavity. Here the exhaust of hotter air takes place along the receiver vertically. Within the zone comprised between the reflector and the gable, the velocity vectors present a direction and magnitude pattern very similar to the case of the covered collector, with particles moving downwards along the side walls of the gable and ascending along the lower surface of the reflector, which is expected since this is the hotter surface of this domain.

The heat fluxes on the uncovered collector case present lower absolute overall ratios the previous case. The reflector is the component with the highest transfer rates per unit surface i.e. - 296 W/m^2. This value stays considerably below the 720 W/m^2 reported in the previous case. Results are represented in figure 5.

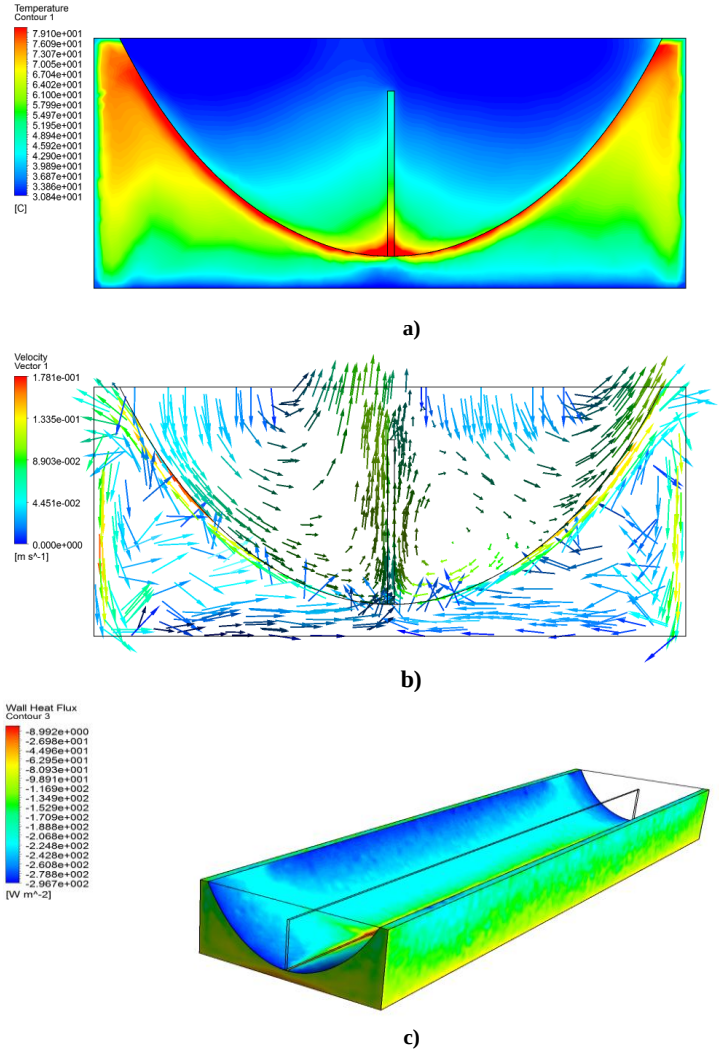

Fig. 5 – Calculated temperature contours (a) and velocity vectors (b) at the plane y=1000 mm and heat flux (c) contours for case 2.

4.3 Case 3 – Partially covered (no side gables)

As mentioned early, a hybrid solution between the covered and the uncovered collector was simulated in order to investigate a presumably more efficient cooling mechanism of the PV cells than the former. Concerning the temperature contours, this particular configuration show vales of around 65 °C in the zone between the reflector and the glass. The removal of side covers allows the introduction of outside air and its exhaust resulting in the lowering of the cell temperature from 150 °C in the case of the covered collector to 90 °C in this solution – figure 6. This indicates that the cells are being cooled efficiently. In this arrangement, the calculated velocity vectors, show a direction opposite to that found in the case of the covered along the lower surface of the glass. This may be due to the fact that the air intake passing through the area where the side covers were located can cause additional disturbances to the flow in this region. In the case of the cavity below the reflector, no changes are noticed concerning the intensity and the direction of the velocity vectors comparing the two cases.

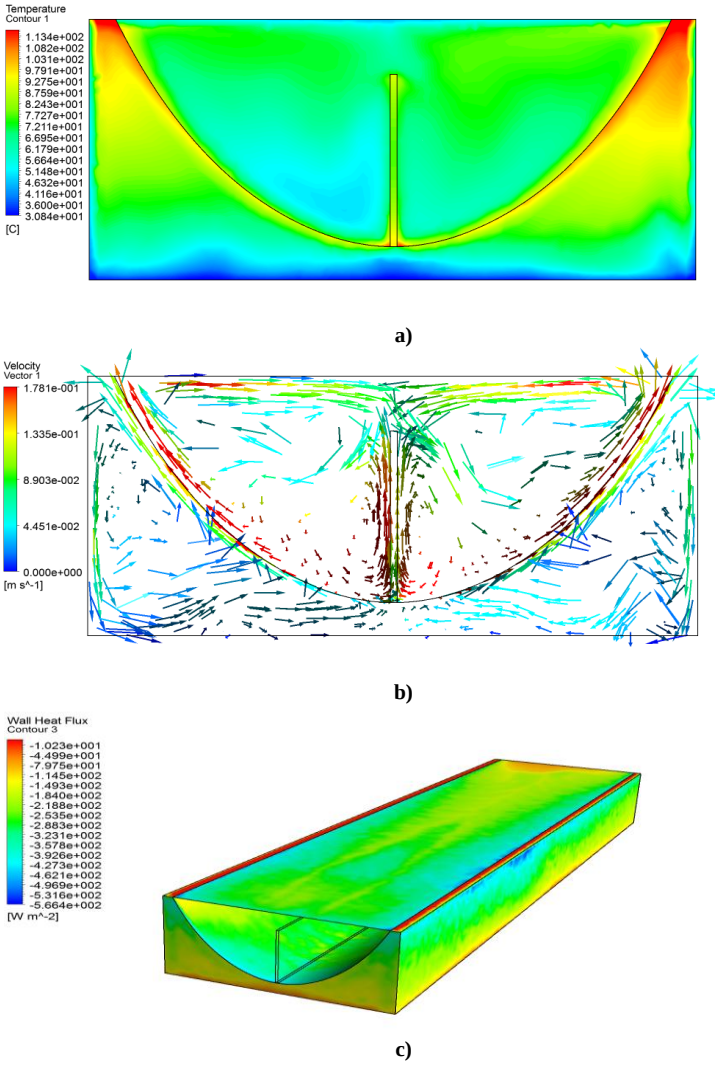

Fig. 6 – Calculated temperature contours (a) and velocity vectors (b) at the plane y=1000 mm and heat flux (c) contours for case 3.

4.4 Case 4 – Partially uncovered (open slot in the side gable)

Simulations were made in a model with openings in the gables and results shown in figure 7. Those are rectangular shaped and induce some air to enter in the collector while keeping the overall equipment structure installed. The slot has a surface equal to 20% of the total of each gable area. The results indicate that the cells reach temperatures between 86 and 106 ° C. This value is about 35% lower than that found for case 1, which shows that ventilation promoted by just opening slots of this dimension allows for lowering cells temperature. Both the part of the receiver close to the base and the reflector have a temperature of 110 ° C - the highest to be reported in the collector. This has to do with the location of the slot in the top of the gable producing a jet of cold air that is more likely to cool the air in the upper of the cavity, just below the glass than the rest of the collector. Regarding the calculated velocity field it needs to be pointed out that below the reflector, residual values are encountered, which helps to explain why higher temperatures are expected to take place in that region, as it was mentioned. This is because heat dissipated by convection, dependent on the flow velocity, is this way decreased. Heat fluxes contours figure shows about 600 W/m^2 of heat loss next to the inlet zone, on the left side of the picture. Meanwhile on the other end, next to the exhaust, values of 36 W/m^2 were reported. This is due to the fact that here the air has been heated to a temperature close to the collector surface which indicates an efficient PV cell cooling mechanism.

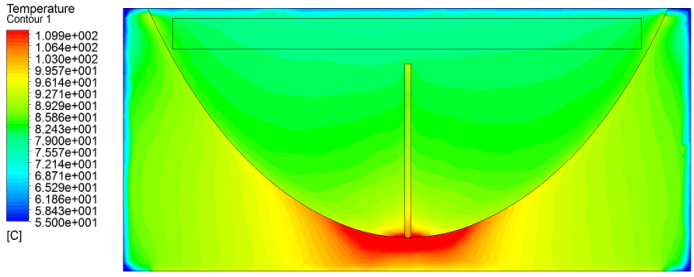

a)

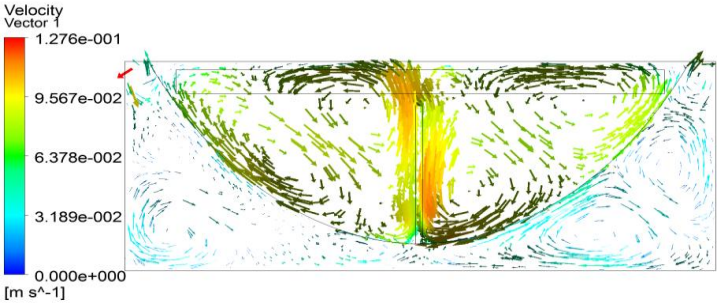

b)

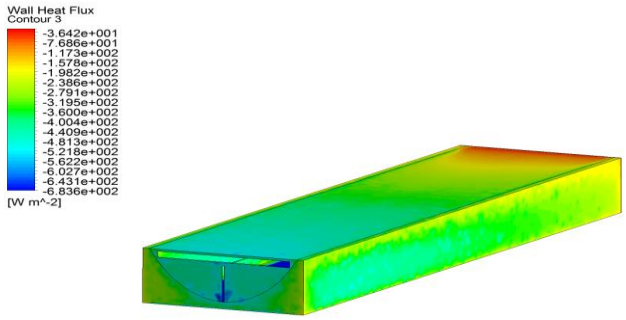

c)

Fig. 7 – Calculated temperature contours (a) and velocity vectors (b) at the plane y=1000 mm and heat flux (c) contours for case 4.

5. Conclusion

The electric output of PV cells is sensitive to their working temperature. Simulations were carried out on four prototypes of concentrating using bifacial collector. Some conclusions can be drawn about the thermal performance of each configuration studied.

The temperature of the cells decreases as the protections are removed from the collector. In the case of a completely airtight collector, equipped with glass and side covers, the cell´s working temperature reaches 150 °C. Concerning cell operating conditions, the optimal solution corresponds to the configuration in which both

the glass and the side protections are eliminated. In this case, the maximum temperature reaches 79ºC, which corresponds to a 47% reduction from a collector with a completely closed collector.
The case where a slot is opened in one of the gables is a solution that enables better cooling of the cells compared to the case where fully closed collector was studied while still protecting the receiver and reflector from the weather. Different opening geometries and locations in the gable need to be investigated, though, in order to optimize the cooling of the collector.
There is, therefore, a direct relationship between the portion of the collector that is not covered and the decrease in the operating temperature of the cells.
Although the glass and gables act like a mass transfer barrier restricting the desired cells heat dissipation, concerns about the protection against mechanical and chemical agents (dirt, rain or wind) arise because of the potential collector damage and, as a result, decreases efficiency. However, a substantial reduction in the collector overall temperature was achieved just by removing minor areas of this components. A heat sink is a possibility to further dissipate heat.

6. References

Alizadeh H., Ghasempour R., Shafii M., Ahmadi M., Yan W., Nazari M., 2018. Numerical simulation of PV cooling by using single turn pulsating heat pipe. International Journal of Heat and Mass Transfer, 127, 203–208.

Çengel, Y. A., 2002. Heat Transfer: A Practical Approach, 2ª Edition, McGraw-Hill.

Du, Y., 2017. Advanced thermal management of a solar cell by a nano-coated heat pipe plate: A thermal assessment. Energy Conversion and Management, 134, 70-76.

Gomes, J., Davidsson H., Christian, G., Stefan, M., Karlsson, B., 2012. Testing bifacial PV cells in symmetric and asymmetric concentrating CPC collectors. Engineering. doi:10.4236/eng.2012

Kasaeian, A., Khanjari, Y., Golzari, S., Mahian, O., Wongwises S., 2017. Effects of forced convection on the performance of a photovoltaic thermal system: An experimental study. Experimental Thermal Fluid Science, 85, 13–21.

Li, W., Paul, M. C., Sellami, N., Mallick, T. K., Knox, A. R., 2016. Experimental and numerical investigation of thermal performance of a crossed compound parabolic concentrator with PV cell. 12th International Conference on Heat Transfer, Fluid Mechanics and Thermodynamics.

Li, Z., 2007. Characteristics of Buoyancy-Driven Natural Ventilation through Horizontal Openings. Ph.D. Thesis. Aalborg University.

Mehrdad, K., Salati, H., Egelioglu, F., Faghiri, A., Tarabishi, J., Babadi, S., 2014. A Review of Solar Photovoltaic Concentrators. International Journal of Photoenergy. Article ID 958521, 17 pages, doi:10.1155/2014/958521.

Spentzos, A., 2005. CFD Analysis of 3D Dynamic Stall. Ph.D. Thesis. Glasgow University.

Sun, J., Shi, M., 2009. China Ser. E-Technol. Sci. 52, 3514. https://doi.org/10.1007/s11431-009-0242-x

Versteeg, H. K., Malasasekera, W., 2007. An Introduction to Computational Fluid Dynamics – The Finite Volume Method. Second edition. Parson Education Limited.

Wu, S., Chen, C., Xiao, L., 2018. Heat transfer characteristics and performance evaluation of water-cooled PV/T system with cooling channel above PV panel. Renewable Energy 125, 936-946.